A Vibrating-String Model for Closed-Loop Wave Transmission and Reflection Between the Aorta and Periphery

Zhili Hao
Department of Mechanical and Aerospace Engineering,
Old Dominion University,
Norfolk, VA 23464
e-mail: zlhao@odu.edu

A tube-load model is used to reconstruct aortic pressure waveform from peripheral pressure waveform. Yet, the reconstructed aortic pressure waveform is greatly affected by load impedance used. In this work, a vibrating-string model for closed-loop wave transmission and reflection between the aorta and periphery is developed to examine the roles of all the parameters involved in aortic pressure waveform. The arterial pulsatile wave theory gives rise to the standard one-dimensional wave equation for a vibrating string. A vibrating-string model based on radial displacement of the arterial wall is developed to relate aortic pressure waveform to peripheral pressure waveform, relate load impedance to input impedance, and derive theoretical expressions for associated clinical indices. The vibrating-string model is extended to incorporate blood velocity and is further connected to the left ventricle (LV) to study the role of the LV in aortic pressure waveform. The difference between the vibrating-string model and the tube-load model is also examined. Load impedance is identified as an indispensable independent parameter for reconstruction of aortic pressure waveform with accuracy, and its physiologically realistic harmonic dependence can only be obtained from the measured input impedance. The derived expressions for clinical indices interpret some clinical findings and underscore the role of harmonics in clinical indices. Some misconceptions in the tube-load model are revealed, including load impedance and characteristic impedance. This work clarifies the role of harmonics-dependence of load impedance and harmonics of aortic pressure waveform in determining clinical indices. [DOI: 10.1115/1.4062078]

Keywords: wave transmission and reflection, vibrating string, load impedance, input impedance, harmonics-dependence, aortic pressure waveform, arterial geometries, and properties

1 Introduction

As compared with peripheral pressure waveform, aortic pressure waveform is more relevant to the left ventricle (LV) function but is difficult and costly to measure [1,2]. Therefore, one-dimensional (1D) models for pulsatile wave propagation in the arterial tree have been developed to reconstruct aortic pressure waveform from measured peripheral pressure waveform [1–7]. Generally speaking, there are two types of 1D models: distributed 1D model and tube-load model [2]. The distributed 1D model includes the arterial tree network (e.g., a large number of arterial segments and bifurcations), and thus involves great computational complexity and has not been extensively used to reconstruct aortic pressure waveform [2]. Built upon a transmission-line analogy, the tube-load model offers great computational simplicity and has been extensively employed in reconstructing aortic pressure waveform [3–7]. In the simplest tube-load model, a uniform, lossless tube represents the arterial section between the aorta and periphery (i.e., the measured artery site), and a load at periphery represents the impedance from the rest arteries and termination [2].

Aortic pressure waveform is characterized by three clinical indices: return time, reflection magnitude, and augmentation index (AI) [2]. As compared with arterial stiffness (i.e., pulse wave velocity (PWV)), these clinical indices have shown their independent values, although they are all thought to be indicative of arterial stiffness [2,5]. In essence, AI is a composite indicator of return time and reflection magnitude. Reconstruction of aortic pressure waveform with accuracy is important for accurate estimates of these clinical indices. To improve accuracy in reconstructed aortic pressure waveform, various complexities (e.g., tapered arterial geometry, transmission loss, and different load impedance) have been incorporated into the tube-load model [2–7]. To date, the majority of the studies on the tube-load model have focused on exploring different load impedance to improve accuracy of reconstructed aortic pressure waveform, because load impedance has significant influence on the shape of reconstructed aortic pressure waveform [1–3,5]. In contrast, input impedance at the aorta has been neglected in the studies on the tube-load model [2–7]. While load impedance separates the forward waves from the reflected waves in peripheral pressure waveform, input impedance separates the forward waves from the reflected waves in aortic pressure waveform. As such, there might be some relationship between the two. It is worth noting that there are measured data for input impedance in the literature [8], but no studies have reported on the measured data for load impedance, to the best knowledge of the author.

Westerhof et al. [1] examined the influence of load type in the tube-load model on input impedance. When a pure resistor is used as the load, the tube-load model fails to interpret the measured relation of return time to PWV in clinical studies and matches the measured input impedance in clinical studies. When a three-element Windkessel model is used as the load, the tube-load model can interpret the measured relation of the return time to PWV and provide reasonable input impedance. However, a

Contributed by the Applied Mechanics Division Technical Committee on Dynamics & Control of Structures & Systems (AMD-DCSS) of ASME for publication in the Journal of Engineering and Science in Medical Diagnostics and Therapy. Manuscript received November 18, 2022; final manuscript received March 1, 2023; published online March 24, 2023. Editor: Ahmed Al-Jumaily.

theoretical relation of load impedance to input impedance in the tube-load model was not provided. Neither a pure resistor nor a three-element Windkessel model as the load is capable of reconstructing aortic pressure waveform with accuracy [4,5]. Moreover, both the distributed 1D model [1] and the tube-load model [2–7] fall short of clarifying physical implications underlying the influence of the load type on input impedance and aortic pressure waveform.

Aortic pressure waveform is a collection of harmonics ($n\omega$, with n and ω as the n-th harmonic and the fundamental frequency, respectively,) of the heartbeat and the sum of the forward and reflected pressure waves [1,5]. Lower-level harmonics are sufficient to capture aortic pressure amplitude but are insufficient to accurately capture aortic pressure waveform [9]. Using machine-learning algorithms, a recent study has found that two sets of values for the three-element Windkessel model as the load for lower-level harmonics and higher-level harmonics, respectively, improve accuracy in reconstructed aortic pressure waveform [5]. This manifests harmonic-dependence of load impedance and insufficiency of one three-element windkessel model for representing this harmonic-dependence. Yet, physical implications of harmonic-dependence of load impedance is unclear, and physiologically realistic harmonic-dependence of load impedance is still unfathomable.

To reconstruct aortic pressure waveform with accuracy, it is essential to clarify physical implications of load type and harmonic-dependence of load impedance and examine the relation of load impedance to input impedance. In this work, built upon the standard 1D wave equation [10], a vibrating-string model based on radial displacement of the arterial wall is developed to clarify the entangled relations of the three parameters: load impedance (Z_L), input impedance (Z_0), and harmonics ($n\omega$), in closed-loop wave transmission and reflection between the aorta and periphery, in which input impedance at the aorta is related to load impedance at periphery. Clarification of the entangled relations reveals the role of the three parameters in aortic pressure waveform and its clinical indices. This vibrating-string model is further extended to incorporate blood velocity. Given the identified role of harmonics of aortic pressure waveform in its clinical indices, the vibrating-string model is connected to the LV to study the LV-artery interaction for exploring the relation of aortic pressure waveform to the driving force on the LV and possible affecting factors of harmonics of aortic pressure waveform. A comparison of the vibrating-string model with the tube-load model is also conducted to identify some misconceptions in the tube-load model for reconstruction of aortic pressure waveform.

The rest of the paper is organized as follows: In Sec. 2, the vibrating-string analogy for arterial pulsatile wave propagation is presented to derive equivalent linear density and equivalent tension from arterial properties and geometries. In Sec. 3, a vibrating-string model based on radial wall displacement is developed to relate aortic pressure waveform to peripheral pressure waveform and relate load impedance to aortic input impedance. Afterwards, return time and reflection magnitude at the aorta is related to both input impedance and load impedance. By relating the theoretical input impedance to the measured input impedance in clinical studies, physiologically realistic harmonic-dependence of load impedance is revealed. The vibrating-string model is extended to incorporate blood velocity. By connecting the vibrating-string model to the LV, a lumped-element mechanical model for the LV-artery interaction is created to relate the driving force on the LV to aortic pressure waveform and explore possible affecting factors of harmonics of aortic pressure waveform. In Sec. 4, the difference between the tube-load model and the vibrating-string model is examined. In Sec. 5, independent parameters and dependent parameters are identified in closed-loop wave transmission and reflection between the aorta and periphery, revealing that load impedance is an indispensable independent parameter for reconstruction of aortic pressure waveform with accuracy, and its physiologically realistic harmonic-dependence can only be obtained from the measured input impedance; and input impedance is a dependent parameter and is determined by load impedance and arterial properties and geometries. The derived expressions for clinical indices and their calculated values, based on the measured harmonics of aortic pressure and blood flow waveforms in the literature [8], interpret some clinical findings and underscore the role of harmonics of aortic pressure waveform in determining its clinical indices. With the vibrating-string model, physical implications of load type and harmonic-dependence of load impedance are made evident. Some misconceptions in the tube-load model become conspicuous. Section 6 summarizes key insights on reconstruction of aortic pressure waveform and its associated physical implications.

2 Vibrating-String Analogy for Pulsatile Wave Propagation in an Artery

In this section, the theory of pulsatile wave propagation in an artery is briefly presented to obtain the standard 1D wave equation for pulsatile parameters in an artery [10]. By comparing this equation with the wave equation for a vibrating string, equivalent tension and equivalent linear density for an artery are related to arterial properties and geometries.

2.1 Pulsatile Wave Propagation in an Artery. As shown in Fig. 1, the arterial wall is assumed to be a thin-walled tube and has two geometrical parameters: thickness h and radius a at diastolic blood pressure (DBP). The arterial wall undergoes radial displacement $\eta(x,t)$ during a pulse cycle. Blood is assumed to be incompressible, Newtonian fluid, and undergo laminar flow. There are three pulsatile parameters in blood flow: radial blood velocity $w(r,x,t)$ and axial blood velocity $u(r,x,t)$, and pulsatile pressure $\Delta p(x,t)$. Each pulsatile parameter is a collection of harmonics ($n\omega$) of the heartbeat. When the wavelength of pulsatile pressure is well below the arterial radius [11], pulsatile pressure does not vary in the radial direction.

The governing equations of blood flow in an artery include the continuity equation and the Navier–Stokes equations in the radial (r-axis) and axial (x-axis) directions [11]

$$\frac{\partial w}{\partial r}+\frac{w}{r}+\frac{\partial u}{\partial x}=0 \tag{1a}$$

$$\rho_b\frac{\partial w}{\partial t}=-\frac{\partial \Delta p}{\partial r}+\mu\left(\frac{\partial^2 w}{\partial r^2}+\frac{1}{r}\frac{\partial w}{\partial r}-\frac{w}{r^2}+\frac{\partial^2 w}{\partial x^2}\right) \tag{1b}$$

$$\rho_b\frac{\partial u}{\partial t}=-\frac{\partial \Delta p}{\partial x}+\mu\left(\frac{\partial^2 u}{\partial r^2}+\frac{1}{r}\frac{\partial u}{\partial r}+\frac{\partial^2 u}{\partial x^2}\right) \tag{1c}$$

where ρ_b and μ denote the blood density and viscosity, respectively. The solution to Eq. (1) is the wave expressions for the nth harmonic of w, u, and Δp [11]

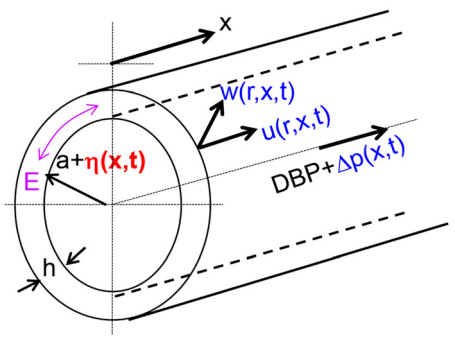

Fig. 1 Schematic of the arterial wall and blood flow in it and the associated geometries and pulsatile parameters

$$w = \left[-\Delta p_0 \frac{\beta_0^2 r}{2\mu\alpha_0^2} + B\frac{\beta_0}{\alpha_0 J_0(\alpha_0)} J_1(\alpha_0 r/a)\right] \cdot e^{i(n\omega t - k_n x)} \tag{2a}$$

$$u = \left[-\Delta p_0 \frac{\beta_0 a}{\mu\alpha_0^2} + B\frac{J_0(\alpha_0 r/a)}{J_0(\alpha_0)}\right] \cdot e^{i(n\omega t - k_n x)} \tag{2b}$$

$$\Delta p = \Delta p_0 \cdot e^{i(n\omega t - k_n x)} \tag{2c}$$

where $\alpha_0^2 = i^3\alpha^2$ with $\alpha = a\sqrt{\rho_b n\omega/\mu}$ being the Womersley number and $\beta_0 = ian\omega/c = i\beta$ [11]; $k_n = n\omega/c_n$ is the nth wave number; and c_n is the nth wave velocity. Note that Δp_0 and B are two constant unknowns.

The governing equations for the arterial wall include its equilibrium equation in the circumferential direction and two no-slip conditions at the blood-wall interface, which involve the three pulsatile parameters in blood flow [10]

$$0 = \Delta p - Eh\frac{\eta}{a^2} \tag{3a}$$

$$w_{r=a} = \frac{\partial \eta}{\partial t} \tag{3b}$$

$$u_{r=a} = 0 \tag{3c}$$

where E denotes the circumferential elasticity of the arterial wall. Note that axial wall displacement is neglected since it has no effect on pulsatile pressure, blood velocity, and radial wall displacement [10]. The wave expression for the nth harmonic of $\eta(x,t)$ can be written as

$$\eta = \eta_0 \cdot e^{i(n\omega t - k_n x)} \tag{4}$$

Substituting Eqs. (2) and (4) into Eq. (3) gives rise to the following 3×3 matrix equation with a vector of the three constant unknowns of Δp_0, B, and η_0

$$\begin{bmatrix} -\frac{\beta_0 a}{\mu\alpha_0^2} & 1 & 0 \\ -\frac{\beta_0^2 a}{2\mu\alpha_0^2} & \frac{1}{2}\beta_0 F_{10} - in\omega & \\ 1 & & 0 - \frac{Eh}{a^2} \end{bmatrix} \begin{Bmatrix} \Delta p_0 \\ B \\ \eta_0 \end{Bmatrix} = \begin{Bmatrix} 0 \\ 0 \\ 0 \end{Bmatrix} \tag{5}$$

where F_{10} is a fluid-loading term, is harmonics-dependent, and takes complex values

$$F_{10} = \frac{2J_1(\alpha_0)}{\alpha_0 J_0(\alpha_0)} \text{ (harmonics-dependent, complex)} \tag{6}$$

Based on Eq. (5), the nth wave velocity of the four pulsatile parameters is

$$c_n = c_0\sqrt{(1 - F_{10})} \quad \text{with} \quad c_0 = \text{PWV} = \sqrt{\frac{Eh}{2\rho_b a}} \tag{7}$$

Note that c_0 is the same as PWV in clinical studies and is independent of harmonics. Given the harmonics-dependence of F_{10}, the wave velocity varies with harmonics.

Excited by the LV, pulsatile pressure $\Delta p(x,t)$ propagates from the aorta to periphery and experiences wave reflection

$$\Delta p(x,t) = \sum_n (A_n e^{-ik_n x} + B_n e^{ik_n x}) e^{in\omega t} \tag{8a}$$

where A_n and B_n denote the nth forward and reflected pressure waves, respectively. Pulsatile pressure gives rise to radial wall displacement $\eta(x,t)$, blood flow rate $Q(x,t)$, and wall shear stress $\tau_w(x,t)$ [10]

$$\eta(x,t) = \frac{a^2}{Eh}\sum_n \left(A_n e^{-ik_n x} + B_n e^{ik_n x}\right) e^{in\omega t} \tag{8b}$$

$$Q(x,t) = u(x,t)\cdot \pi a^2 = \frac{\pi a^2}{\rho_b}\sum_n \frac{1 - F_{10}}{c_n}\left(A_n e^{-ik_n x} - B_n e^{ik_n x}\right) e^{in\omega t} \tag{8c}$$

$$\tau_w(x,t) = \mu\frac{\partial u}{\partial r}\Big|_{r=a} = -\frac{a}{2}\sum_n \frac{in\omega F_{10}}{c_n}\left(A_n e^{-ik_n x} - B_n e^{ik_n x}\right) e^{in\omega t} \tag{8d}$$

where $u(x,t)$ is the blood velocity averaged across the lumen. While wave reflection augments pulsatile pressure and radial wall displacement, it reduces blood velocity and wall shear stress.

2.2 Standard One-Dimensional Wave Equation for Pulsatile Wave Propagation in an Artery. For simplicity, the subscript n for harmonics is omitted here. Comparison of the second-order derivatives of $\eta(x,t)$ with respect to t and x, respectively, provides the following equation

$$\frac{\partial^2 \eta}{\partial t^2} = c^2\frac{\partial^2 \eta}{\partial x^2} \tag{9}$$

The above equation can be further rewritten as

$$\rho_b \pi a^2 \frac{\partial^2 \eta}{\partial t^2} = \frac{Eh\pi a}{2}(1 - F_{10})\frac{\partial^2 \eta}{\partial x^2} \tag{10a}$$

The governing equation for a vibrating string with linear density ρ_L and tension T is given as [12]

$$\rho_L \frac{\partial^2 \eta}{\partial t^2} = T\frac{\partial^2 \eta}{\partial x^2} \quad \text{with} \quad c = \sqrt{T/\rho_L} \quad \text{(wave velocity)} \tag{10b}$$

Comparison of Eqs. (10*a*) and (10*b*) indicates that pulsatile wave propagation in an artery is equivalent to wave propagation in a vibrating string with cross section area πa^2, density ρ_b, and tension T

$$\rho_L = \rho_b \pi a^2 \quad \text{and} \quad T = \frac{\pi Eh}{2}a(1 - F_{10}) \tag{11}$$

While T is harmonics-dependent, ρ_L is harmonics-independent. Note that $1-F_{10}$ is harmonics-dependent at small arteries, such as the carotid artery and the radial artery, and $1-F_{10} \cong 1$ is harmonics-independent at the aorta, due to its large size.

3 A Vibrating-String Model for Closed-Loop Wave Transmission and Reflection Between the Aorta and Periphery

According to Eqs. (3*a*) and (8), radial wall displacement waveform is identical to pressure waveform. Given that radial wall displacement carries evident physical implication to wave transmission and reflection in the context of the 1D wave propagation, radial wall displacement is analyzed here, instead of pulsatile pressure. By modeling the aorta-periphery section as a uniform vibrating-string, aortic radial wall displacement waveform is related to peripheral radial wall displacement waveform, and input impedance is related to load impedance. Additionally, return time and reflection magnitude at the aorta is related to both input impedance and load impedance. The role of harmonics of radial wall displacement on return time and reflection magnitude is identified. By relating the theoretical input impedance to the

measured input impedance in clinical studies, physiological realistic harmonics-dependence of load impedance is revealed. The analysis on radial wall displacement is extended to blood velocity as equivalent transverse displacement, and the input power at the aorta for radial wall displacement and blood velocity is derived. By connecting the vibrating-string model to the LV, the LV-artery interaction is analyzed to relate driving force on the LV to aortic pressure waveform.

3.1 Relation of Aortic Radial Wall Displacement Waveform to Peripheral Radial Wall Displacement Waveform. Figure 2 shows the vibrating-string model for the aorta-periphery section, which is connected to the rest arteries and termination. The arterial section between $x \in (0, L)$ is treated as a uniform vibrating-string with equivalent linear density ρ_L and equivalent tension T. The radial wall displacements at the aorta and at periphery are $\eta(0,t)$ and $\eta(L,t)$, respectively. Part of $\eta(L,t)$ further propagates into the rest arteries and ends at termination (with unknown boundary conditions). The nth wave velocity is complex with real part $c_0 Re(\sqrt{1-F_{10}})$ and imaginary part $c_0 Im(\sqrt{1-F_{10}})$. Then, the nth wave transmits in the positive x-axis involves wave transmission k_n and transmission loss γ_n

$$e^{-ik_n x}e^{-\gamma_n x} \text{ with } k_n = \frac{n\omega}{c_0 \mathrm{Re}\left(\sqrt{1-F_{10}}\right)} \text{ and } \gamma_n = \frac{n\omega}{c_0 \mathrm{Im}\left(\sqrt{1-F_{10}}\right)} \tag{12}$$

Except arterial geometries and properties (i.e., a, h, L, E, μ, and ρ_b) and c_0, $\eta(x,t)$ and other parameters (i.e., load impedance, input impedance, reflection coefficient, wave velocity, and F_{10}) involved in this section are all harmonics-dependent.

We derive the mathematical expression for the nth aortic radial wall displacement $\eta_{an}(t)=\eta_n(0,t)$ in terms of the nth peripheral radial wall displacement $\eta_{pn}(t)=\eta_n(L,t)$. The nth radial wall displacement $\eta_n(x,t)$ at x-position is expressed as

$$\eta_n(x,t) = (A_n e^{-ik_n x}e^{-\gamma_n x} + B_n e^{ik_n x}e^{\gamma_n x})e^{in\omega t} \tag{13a}$$

where A_n and B_n denote the amplitudes of the nth forward and reflected waves at the aorta, respectively. The nth driving force $F_n(x,t)$ is written as

$$F_n(x,t) = -T\partial\eta_n/\partial x = \rho_L c_n in\omega(A_n e^{-ik_n x}e^{-\gamma_n x} - B_n e^{ik_n x}e^{\gamma_n x})e^{in\omega t} \tag{13b}$$

The nth mechanical impedance Z_n is defined as [12]

$$Z_n(x) = \frac{F_n}{\partial\eta_n/\partial t} = \rho_L c_n \frac{(A_n e^{-ik_n x}e^{-\gamma_n x} - B_n e^{ik_n x}e^{\gamma_n x})}{(A_n e^{-ik_n x}e^{-\gamma_n x} + B_n e^{ik_n x}e^{\gamma_n x})} \tag{14}$$

Based on Eq. (14), the nth characteristic impedance Z_{cn} is given as [12]

$$Z_{cn} = \rho_b c_n \pi a^2 = \rho_b c_0 \pi a^2 \sqrt{(1-F_{10})} \tag{15}$$

According to Eq. (13a), the nth peripheral radial wall displacement $\eta_{pn}(t)$ becomes

$$\eta_{pn}(t) = \eta_n(L,t) = (A_n e^{-ik_n L}e^{-\gamma_n L} + B_n e^{ik_n L}e^{\gamma_n L})e^{in\omega t} = (\eta_{pfn} + \eta_{pbn})e^{in\omega t} \tag{16a}$$

where η_{pfn} and η_{pbn} denote the amplitudes of the nth forward and reflected waves at periphery, respectively, and their ratio represents the nth reflection coefficient Γ_n at $x=L$

$$\frac{\eta_{pbn}}{\eta_{pfn}} = \Gamma_n = \Omega_n \cdot e^{i\theta_n} \quad (\theta_n < 0) \tag{16b}$$

where Ω_n is a real number, and $\theta_n < 0$, because η_{pfn} is ahead of η_{pbn}. The nth load impedance Z_{Ln} is related to Γ_n by

$$Z_{Ln} = Z_{cn}\frac{1-\Gamma_n}{1+\Gamma_n} \quad \text{or} \quad \Gamma_n = \Omega_n e^{i\theta_n} = \frac{Z_{cn}-Z_{Ln}}{Z_{cn}+Z_{Ln}} \tag{17}$$

The nth radial wall displacement at x-position can be expressed in terms of η_{pfn} and Γ_n

$$\eta_n(x,t) = \eta_{pfn}(e^{i(k_n L - x)}e^{\gamma_n(L-x)} + \Omega_n e^{i\theta_n}e^{-ik_n(L-x)}e^{-\gamma_n(L-x)})e^{in\omega t} \tag{18}$$

According to Eqs. (16b) and (18), $\eta_{an}(t)$ at the aorta can be derived from $\eta_{pn}(t)$

$$\eta_{an}(t) = (\eta_{afn} + \eta_{abn})e^{in\omega t} = \frac{e^{ik_n L}e^{\gamma_n L} + \Gamma_n e^{-ik_n L}e^{-\gamma_n L}}{(1+\Gamma_n)}\eta_{pn}(t) \tag{19}$$

Note that Eq. (19) is identical to the one in the tube-load model [4].

3.2 Relation of Input Impedance to Load Impedance. According to Eq. (14), the nth input impedance Z_{0n} is related to Γ_n and Z_{Ln} by

$$\begin{aligned} Z_{0n} &= Z_{cn}\frac{A_n - B_n}{A_n + B_n} \\ &= Z_{cn}\frac{Z_{cn}(e^{2ik_n L}e^{2\gamma_n L} - 1) + Z_{Ln}(e^{2ik_n L}e^{2\gamma_n L} + 1)}{Z_{cn}(e^{2ik_n L}e^{2\gamma_n L} + 1) + Z_{Ln}(e^{2ik_n L}e^{2\gamma_n L} - 1)} \\ &= Z_{cn}\frac{e^{2ik_n L}e^{2\gamma_n L} - \Gamma_n}{e^{2ik_n L}e^{2\gamma_n L} + \Gamma_n} \\ &= Z_{cn}\frac{e^{2\gamma_n L} - \Omega_n{}^2 e^{-2\gamma_n L} + 2\Omega_n\{\sin(2k_n L - \theta_n)\}i}{e^{2\gamma_n L} + \Omega_n{}^2 e^{-2\gamma_n L} + 2\Omega_n\{\cos(2k_n L - \theta_n)\}} \end{aligned} \tag{20}$$

Equation (20) indicates dependence of wave reflection at the aorta on wave reflection at periphery and closes the loop on wave transmission and reflection between the aorta and periphery. In order to relate Z_{0n} to the corresponding measured input impedance in clinical studies later on, the above nth theoretical input impedance is further written as

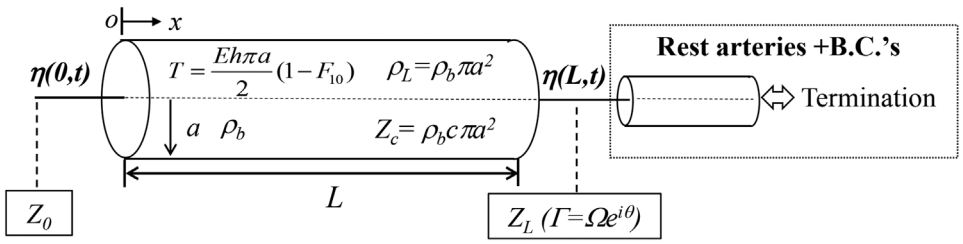

Fig. 2 An equivalent vibrating-string model for pulsatile wave propagation in the arterial tree (Note: dependence of some parameters on harmonics (or *n*) is omitted for simplicity)

$$Z_{0n} = Z_{cn}\frac{A_n - B_n}{A_n + B_n} = Z_{cn}{G_n}^{-1}e^{-i\phi_n} \quad \text{with}$$
$$\frac{Z_{0n}}{Z_{cn}} = \frac{A_n - B_n}{A_n + B_n} = {G_n}^{-1}e^{-i\phi_n} \tag{21}$$

where ${G_n}^{-1}e^{-i\phi_n}$ is defined as the nth normalized input impedance. The phase between the driving force and the radial wall velocity for the nth harmonic becomes

$$\text{phase}_n = a\tan\frac{2\Omega_n\{\sin(2k_nL - \theta_n)\}}{e^{2\gamma_nL} - {\Omega_n}^2e^{-2\gamma_nL}} = -\phi_n \tag{22}$$

As will be seen later on, since $\phi_n < 0$ for the first three harmonics ($n = 1, 2, 3$), the driving force is ahead of the radial wall velocity for these harmonics.

Based on Eq. (20), the nth reflection coefficient and load impedance are related to the nth normalized input impedance by

$$\Gamma_n = \Omega_n \cdot e^{i\theta_n} = e^{2ik_nL}e^{2\gamma_nL}\frac{G_ne^{i\phi_n} - 1}{G_ne^{i\phi_n} + 1} \tag{23a}$$

$$Z_{Ln} = Z_{cn}\frac{{G_n}^{-1}e^{-i\phi_n}(e^{2ik_nL}e^{2\gamma_nL} + 1) + (1 - e^{2ik_nL}e^{2\gamma_nL})}{{G_n}^{-1}e^{-i\phi_n}(1 - e^{2ik_nL}e^{2\gamma_nL}) + (e^{2ik_nL}e^{2\gamma_nL} + 1)} \tag{23b}$$

Accordingly, the nth reflection coefficient can be obtained from the nth normalized input impedance and wave velocity (i.e., k_n and γ_n), while the nth load impedance can be obtained from the nth normalized input impedance and wave velocity, as well as the nth characteristic impedance.

3.3 Return Time and Reflection Magnitude and Reconstruction of Aortic Radial Wall Displacement Waveform. Based on Eq. (18), the nth radial wall displacement at the aorta is

$$\eta_{an}(t) = \eta_{pfn}e^{ik_nL}e^{\gamma_nL}(1 + \Omega_ne^{i\theta_n}e^{-2ik_nL}e^{-2\gamma_nL})e^{in\omega t} \tag{24}$$

By combining Eqs. (20), (23), and (24), the nth reflection coefficient Γ_{0n} at the aorta is

$$\Gamma_{0n} = \Omega_{0n}e^{i\varphi_n} = \frac{\eta_{abn}}{\eta_{afn}} = \Omega_ne^{i\theta_n}e^{-2ik_nL}e^{-2\gamma_nL} = \frac{G_ne^{i\phi_n} - 1}{G_ne^{i\phi_n} + 1}$$
$$= \frac{G_n^2 - 1 + 2G_n\sin\phi_n i}{G_n^2 + 2G_n\cos\phi_n + 1} \tag{25}$$

The reflection magnitude Ω_{0n} and return time Δt_n of the nth reflected wave at the aorta are

$$\Omega_{0n} = \left|\frac{G_ne^{i\phi_n} - 1}{G_ne^{i\phi_n} + 1}\right| \tag{26a}$$

$$\Delta t_n = \frac{2L}{c_0Re\left(\sqrt{1 - F_{10}}\right)} - \frac{\theta_n}{n\omega} = \frac{-a\tan\dfrac{2G_n\sin\phi_n}{{G_n}^2 - 1}}{n\omega} \tag{26b}$$
$$(q_n < 0 \quad \text{and} \quad f_n < 0)$$

Accordingly, return time varies with harmonics and is affected by the phase of reflection coefficient at periphery, and can be obtained from the input impedance.

Based on Eq. (25), Z_{0n} provides reflection magnitude and phase delay for the nth forward and reflected waves, but it does not contain the harmonics (i.e., amplitude and phases of the first ten harmonics) of the forward waves. In this regard, aortic radial wall displacement waveform carries more physiological information than the input impedance, as illustrated in the expression for aortic radial wall displacement waveform

$$\eta_a(t) = \eta_{af}(t) + \eta_{ab}(t) = \sum_n\frac{2G_ne^{i\phi_n}}{G_ne^{i\phi_n} + 1}\eta_{afn}e^{in\omega t}$$
$$= \sum_n\left(1 + \Omega_ne^{i\theta_n}e^{-2ik_nL}e^{-2\gamma_nL}\right)\eta_{pfn}e^{ik_nL}e^{\gamma_nL}e^{in\omega t} \tag{27}$$

As such, the input impedance and the harmonics of the forward wave need to be treated as two independent parameters for determining aortic radial wall displacement waveform. Alternatively, the normalized input impedance and aortic radial wall displacement waveform can be treated as two independent parameters to determine the harmonics of the forward waves.

Based on Eq. (25), reflection amplitude Ω_{whole} for the whole aortic radial wall displacement waveform is

$$\Omega_{\text{whole}} = \frac{\eta_{ab}(t)}{\eta_{af}(t)} = \frac{\sum_n\dfrac{G_ne^{i\phi_n} - 1}{G_ne^{i\phi_n} + 1}\eta_{afn}e^{in\omega t}}{\sum_n\eta_{afn}e^{in\omega t}}$$
$$= \frac{\sum_n\Omega_ne^{i\theta_n}e^{-\gamma_nL}e^{-ik_nL}\eta_{pfn}e^{in\omega t}}{\sum_n\eta_{pfn}e^{ik_nL}e^{\gamma_nL}e^{in\omega t}} \tag{28}$$

Evidently, harmonics of the forward waveform affects reflection amplitude for the whole waveform and AI, which is defined as the ratio of augmented pressure to pulsatile pressure (see Fig. 7).

Based on Eq. (19), aortic radial wall displacement waveform can be reconstructed from peripheral radial wall displacement waveform, without knowing harmonics of the forward waveform

$$\eta_a(t) = \sum_n\frac{e^{ik_nL}e^{\gamma_nL} + \Gamma_ne^{-ik_nL}e^{-\gamma_nL}}{(1 + \Gamma_n)}\eta_{pn}(t)$$
$$= \sum_n\frac{2G_ne^{i\phi_n}e^{ik_nL}e^{\gamma_nL}}{G_ne^{i\phi_n} + 1 + e^{2ik_nL}e^{2\gamma_nL}(G_ne^{i\phi_n} - 1)}\eta_{pn}(t) \tag{29}$$

The known values of k_n and γ_n and L are insufficient to reconstruct aortic radial wall displacement waveform from its peripheral counterpart. Either normalized input impedance or reflection coefficient at periphery is needed. Harmonics-dependence of normalized input impedance (or harmonics-dependence of reflection coefficient at periphery) translates to 20 unknown values in Eq. (29) if only the first ten harmonics are used.

3.4 Relation of the Theoretical Input Impedance to the Measured Input Impedance in Clinical Studies. In clinical studies, the nth characteristic impedance is defined as [8]

$$Z_{\text{cn\_meas}} = \frac{\Delta p_n}{Q_n} = \frac{\rho_bc_0}{\sqrt{1 - F_{10}}\pi a^2} \tag{30}$$

The subscript *meas* is used for all the parameters used in clinical studies. The nth measured input impedance is expressed as

$$Z_{0n-\text{meas}} = \frac{\Delta p_n}{Q_n} = Z_{cn-a-\text{meas}}\frac{A_n + B_n}{A_n - B_n} = \left(\frac{\rho_bc_0}{\pi a^2}\right)_{\text{aorta}}G_ne^{i\phi_n}$$
$$\text{with} \quad \frac{A_n + B_n}{A_n - B_n} = G_ne^{i\phi_n} \tag{31}$$

Based on Eqs. (3a) and (8), G_n and ϕ_n in Eq. (31) are identical to those in Eq. (21). Comparison of Eq. (20) and Eq. (31) leads to the following expression

$$Z_{0n} = Z_{cn}\frac{\left(\dfrac{\rho_bc_n}{\pi a^2}\right)_{\text{aorta}}}{Z_{0n-\text{meas}}} \tag{32}$$

Table 1 Comparison of the vibrating-string models for radial wall displacement and blood velocity and the tube-load model

	Vibrating-string model		Tube-load model
	Arterial wall	Blood flow	Arterial wall+ blood flow
Governing equation	$\frac{\partial^2\eta}{\partial t^2}=c^2\frac{\partial^2\eta}{\partial x^2}$	$\frac{\partial^2 u}{\partial t^2}=c^2\frac{\partial^2 u}{\partial x^2}$	$-\frac{\partial Q}{\partial x}=\frac{2\pi a^3}{Eh}\frac{\partial \Delta p}{\partial t}$ $-\frac{\partial \Delta p}{\partial x}=\frac{\rho_b}{\pi a^2}\frac{\partial Q}{\partial t}+\frac{8\mu}{\pi a^4}Q$
Transverse displacement	η	u	$\int Q\cdot dt$
Velocity	$\partial\eta/\partial t$	$\partial u/\partial t$	$Q=u\cdot\pi a^2$
Driving force	$-T\partial\eta/\partial x$	$-T\partial u/\partial x$	Δp
characteristic impedance	$\rho_b c_n\pi a^2$	$\rho_b c_n\pi a^2$	$\frac{\rho_b c_0}{\pi a^2\sqrt{1-F_{10}}}$
Input impedance	$\rho_b c_n\pi a^2 G_n^{-1}e^{-i\phi_n}$	$\rho_b c_n\pi a^2 G_n^{-1}e^{-i\phi_n}$	$\frac{\rho_b c_0}{\pi a^2\sqrt{1-F_{10}}}G_n e^{i\phi_n}$
Input power	$\frac{1}{2}\left[\frac{2n\omega\eta_{afn}}{G_n e^{i\phi_n}+1}\right]^2\rho_b c_n\pi a^2 G_n e^{i\phi_n}$	$\frac{1}{2}\left[\frac{2n\omega\eta_{afn}}{G_n e^{i\phi_n}+1}\right]^2 4\pi\rho_b c_n^3 G_n e^{i\phi_n}$	$\frac{1}{2}\left[\frac{2\eta_{afn}}{G_n e^{i\phi_n}+1}\right]^2\frac{4\pi\rho_b c_n^3}{1-F_{10}}G_n e^{i\phi_n}$

3.5 Blood Velocity and Input Power at the Aorta. As shown in Eq. (8), the same pulsatile pressure causes radial wall displacement and blood velocity simultaneously, with both transmitting power from the aorta to periphery. Here, the above-detailed vibrating-string model is extended to incorporate blood velocity. In fact, $\eta(x,t)$ in Eq. (9) can be replaced by $\Delta p(x,t)$ and $u(x,t)$

$$\frac{\partial^2\Delta p}{\partial t^2}=c^2\frac{\partial^2\Delta p}{\partial x^2}\quad\text{and}\quad\frac{\partial^2 u}{\partial t^2}=c^2\frac{\partial^2 u}{\partial x^2}\tag{33}$$

Accordingly, pulsatile pressure, radial wall displacement, and blood velocity are all analogous to transverse displacement in a vibrating string and propagate along the axial direction with the same wave velocity and characteristic impedance. While radial wall displacement is associated with elastic energy transmission through the arterial wall, blood velocity is associated with kinetic energy transmission and mass transport through blood flow.

Based on Eq. (33), blood velocity is equivalent to transverse displacement in the vibrating-string model. Then, blood acceleration $\partial u/\partial t$ is the velocity and the driving force is $-T\partial u/\partial x$. The blood velocity and its driving force for the nth harmonic are written in terms of the nth radial wall displacement in Eq. (13*a*)

$$u_n(x,t)=\frac{2c_n}{a}\left(A_n e^{-ik_n x}e^{-\gamma_n x}+B_n e^{ik_n x}e^{\gamma_n x}\right)e^{in\omega t}\tag{34a}$$

$$F_{n-u}(x,t)=-T\partial u_n/\partial x=\rho_L c_n in\omega\frac{2c_n}{a}\left(A_n e^{-ik_n x}e^{-\gamma_n x}-B_n e^{ik_n x}e^{\gamma_n x}\right)e^{in\omega t}\tag{34b}$$

As transverse displacement, blood velocity is the sum of the forward waves and the reflected waves in Eq. (34*a*). The mechanical impedance and input impedance for blood velocity are the same as those for radial wall displacement, as expressed in Eqs. (14) and (32). Comparison of Eqs. (13*b*) and (34*b*) shows that the driving force for blood velocity is $2c_n/a$ times larger than that for radial wall displacement.

Based on the vibrating-string models for radial wall displacement and blood velocity, the nth input power $P_{n\text{-}\eta}$ at the aorta for the arterial wall and the nth input power $P_{n\text{-}u}$ at the aorta for blood flow are given by

$$P_{n-\eta}=\frac{1}{2}\left(\frac{\partial\eta_n}{\partial t}\right)^2 Z_{0n}=\frac{1}{2}\left[\frac{2n\omega\eta_{afn}}{G_n e^{i\phi_n}+1}\right]^2\rho_b c_n\pi a^2 G_n e^{i\phi_n}\tag{35a}$$

$$P_{n-u}=\frac{1}{2}\left(\frac{\partial u_n}{\partial t}\right)^2 Z_{0n}=\frac{1}{2}\left[\frac{2n\omega\eta_{afn}}{G_n e^{i\phi_n}+1}\right]^2 4\pi\rho_b c_n^3 G_n e^{i\phi_n}=\frac{4c_n^2}{a^2}P_{n-\eta}\tag{35b}$$

The total nth input power at the aorta is the sum of $P_{n\text{-}\eta}$ and $P_{n\text{-}u}$. Given $P_{n\text{-}u}\gg P_{n\text{-}\eta}$, blood flow is the dominant carrier of power transmission. Although the amplitudes of the harmonics at the aorta drop greatly with higher n-level [1,8,10], harmonics-dependent input power might indicate that the contribution of higher n-level harmonics to the input power is non-negligible. Table 1 summarizes the vibrating-string models for radial wall displacement and blood velocity and their comparison with the tube-load model, as described later on.

3.6 Left Ventricle-Artery Interaction for Relating Driving Force on the Left Ventricle to Aortic Pressure Waveform. The LV excites pulsatile waves in the arterial tree and is expected to play a role in harmonics of aortic pressure waveform. As shown in Fig. 3, the LV is modeled as a second-order dynamic system and is connected to the aortic end of the arterial tree. The arterial tree interferes with the response of the LV to its driving force. As to the LV, the arterial tree and termination are condensed to the input impedance, and become a spring and a damper in parallel, with $Im(Z_{0n})$ and $Re(Z_{0n})$ as the spring stiffness and the damping coefficient for the nth harmonic, respectively [12]. While $Im(Z_{0n})$ leads to no energy loss to the LV and is a spring, $Re(Z_{0n})$ causes energy absorption by the arterial tree and is a damper. In the lumped-element model for the LV-artery interaction, the input is the driving force on the LV, and the output is radial wall displacement and blood velocity. The driving forces $F_\eta(t)$ and $F_u(t)$ on the LV for radial wall displacement and blood velocity, respectively, can be calculated from radial wall displacement

$$F_\eta(t)=\sum_n in\omega\left\{D+i\left(Mn\omega-\frac{K}{n\omega}\right)+\mathrm{Re}(Z_{0n})+i\,\mathrm{Im}(Z_{0n})\right\}\eta_{an}(t)\tag{36a}$$

$$F_u(t)=\sum_n in\omega\left\{D+i\left(Mn\omega-\frac{K}{n\omega}\right)+\mathrm{Re}(Z_{0n})+i\,\mathrm{Im}(Z_{0n})\right\}\frac{2c_0}{a}\eta_{an}(t)\tag{36b}$$

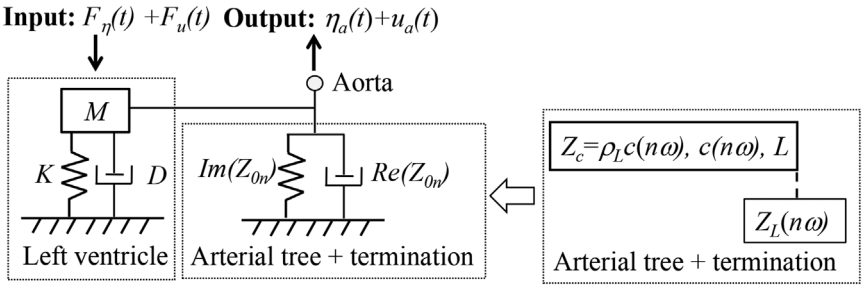

Fig. 3 A lumped-element mechanical model for the LV-artery interaction: the LV is modeled as a second-order dynamic system with mass *M*, spring stiffness *K*, and damping coefficient *D*; and the arterial tree and termination is modeled as a spring (spring stiffness: *Im*(Z_{0n})) and a damper (damping coefficient: *Re*(Z_{0n})) in parallel

where

$$\eta_{an}(t) = \eta_{afn}e^{i\omega t} + \eta_{abn}e^{i\omega t} \quad Z_{0n} = \frac{(\rho_b c_0)^2_{\text{aorta}}}{Z_{0n-\text{meas}}} \tag{37}$$

The input impedance Z_{0n} can be obtained from the measured input impedance. Note that radial wall displacement waveform is identical to pulsatile pressure waveform, and $F_\eta(t)$ and $F_u(t)$ carry the same waveform, with $F_u(t) \gg F_\eta(t)$.

4 Comparison of the Tube-Load Model With the Vibrating-String Model

The difference between the uniform tube-load model and the uniform vibrating-string model is examined here.

4.1 Difference in Governing Equations. For simplicity, the subscript n for harmonics is omitted here. The uniform tube-load model is based on two simplified governing equations for blood flow in an artery: the continuity equation and the axial blood flow equation [2]

$$-\frac{\partial Q}{\partial x} = \frac{\partial A}{\partial t} = C\frac{\partial \Delta p}{\partial t} \tag{38a}$$

$$-\frac{\partial \Delta p}{\partial x} = L\frac{\partial Q}{\partial t} + \frac{2\tau_w}{a} \tag{38b}$$

where Q is blood flow rate; $A = \pi(a+\eta)^2$ is cross section area of the lumen; C and L denote arterial compliance and arterial inductance, respectively [6]

$$C = \frac{2\pi a^3}{Eh}, \quad L = \frac{\rho_b}{\pi a^2} \tag{39a}$$

Note that Eq. (3*a*) is used in the derivation of C. By assuming $\eta(x,t) = 0$, wall shear stress is a function of Q [6]

$$\tau_w = \frac{aR}{2}\cdot Q \quad \text{with} \quad R = \frac{8\mu}{\pi a^4} \tag{39b}$$

Then, substituting Eq. (39*b*) into Eq. (38*b*) leads to

$$-\frac{\partial \Delta p}{\partial x} = L\frac{\partial Q}{\partial t} + RQ \tag{40}$$

Combination of Eqs. (38*a*) and (40) gives rise to

$$\frac{\partial^2 \Delta p}{\partial t^2} + \frac{R}{L}\frac{\partial \Delta p}{\partial t} = c^2_{\text{tube}}\frac{\partial^2 \Delta p}{\partial x^2} \quad \text{with} \quad c_{\text{tube}} = \sqrt{1/(LC)} = c_0 \tag{41}$$

According to Eq. (40), pulsatile wave propagation in an artery is analogous to a transmission line: Q and Δp are equivalent to current and voltage, respectively. Due to the assumption on $\eta(x,t) = 0$, wave velocity c_0 does not vary with harmonics, and damping coefficient R/L is a constant.

Here, we derive the governing equation Eq. (10) for the vibrating-string model from Eq. (38*b*). By substituting Eqs. (8*c*) and (8*d*) into Eq. (38*b*), we can obtain

$$\frac{\partial^2 \Delta p}{\partial t^2} + \frac{in\omega F_{10}}{(1-F_{10})}\frac{\partial \Delta p}{\partial t} = c^2_{\text{tube}}\frac{\partial^2 \Delta p}{\partial x^2} \tag{42a}$$

$$\frac{\partial^2 \Delta p}{\partial t^2} = \frac{Eh(1-F_{10})}{2\rho_b a}\frac{\partial^2 \Delta p}{\partial x^2} \tag{42b}$$

When $\eta(x,t) \neq 0$, wall shear stress is harmonics-dependent and is not linearly proportional to Q. Therefore, damping coefficient is not a constant in Eq. (42*a*). As shown in Eq. (42*b*), the contribution of wall shear stress to the wave propagation can be included into the x-derivative of pulsatile pressure, leading to a complex, harmonics-dependent wave velocity.

4.2 Difference in Characteristic Impedance, Load Impedance, and Input Impedance. In the tube-load model, the characteristic impedance is defined as [2,3]

$$Z_{c-\text{tube}} = \frac{\Delta p}{Q} = \sqrt{\frac{L}{C}} = \frac{\rho_b \cdot c_0}{\pi a^2} \tag{43}$$

This definition is the same as characteristic impedance, Eq. (30), in clinical studies, except that F_{10} is omitted. This characteristic impedance is harmonics-independent. Two types of load impedance used in the tube-load model are a pure resistor and a three-element Windkessel model [3,4]

$$Z_{L-\text{tube}} = R_L \quad (\text{pure resistor}) \tag{44a}$$

$$Z_{Ln-\text{tube}} = Z_{c-\text{tube}} + \frac{R_L}{1+n\omega CR_L i} \quad (\text{three-element Windkessel model}) \tag{44b}$$

While a pure resistor gives rise to harmonics-independent load impedance, a three-element Windkessel model stipulates harmonics-dependence of load impedance. Consequently, reflection coefficient at $x = L$ is written as

$$\Gamma_{\text{tube}} = \frac{R_L - Z_{c-\text{tube}}}{R_L + Z_{c-\text{tube}}} \tag{45a}$$

Table 2 Comparison between the uniform vibrating-string model for radial wall displacement and the uniform tube-load model with a three-element Windkessel model as the load

	Tube-load model	Vibrating-string model
Driving force	Δp_n	$F_n = -T_n \partial \eta_n / \partial x$
Velocity	Q_n	$\partial \eta_n / \partial t$
Arterial compliance	$C = \dfrac{2\pi a^3}{Eh}$	$1/T_n = \left[\dfrac{\pi Eh}{2} a(1-F_{10})\right]^{-1}$
Arterial inductance	$L = \dfrac{\rho_b}{\pi a^2}$	$c_n = c_0\sqrt{(1-F_{10})}$
Wave velocity	$c_{\text{tube}} = c_0$	$c_n = c_0\sqrt{(1-F_{10})}$
Damping coefficient	$\dfrac{8\mu}{\rho_b a^2}$	$\dfrac{in\omega F_{10}}{(1-F_{10})}$
Characteristic impedance	$Z_{c-\text{tube}} = \dfrac{\rho_b \cdot c_0}{\pi a^2}$	$Z_{cn} = \rho_b c_0 \sqrt{(1-F_{10})}\pi a^2$
Load impedance	$Z_{Ln-\text{tube}} = Z_{c-\text{tube}} + \dfrac{R_L}{1+jn\omega C}$	$Z_{Ln} = Z_{cn}\dfrac{G_n^{-1}e^{-i\phi_n}(e^{2ik_nL}e^{2\gamma_nL}+1)+(1-e^{2ik_nL}e^{2\gamma_nL})}{G_n^{-1}e^{-i\phi_n}(1-e^{2ik_nL}e^{2\gamma_nL})+(e^{2ik_nL}e^{2\gamma_nL}+1)}$
Reflection coefficient	$\Gamma_{n-\text{tube}} = \dfrac{R_L}{2Z_{c-\text{tube}}+R_L+2Z_{c-tube}n\omega R_L \text{Ci}}$	$\Gamma_n = e^{2ik_nL}e^{2\gamma_nL}\dfrac{G_n e^{i\phi_n}-1}{G_n e^{i\phi_n}+1}$
Input impedance	$Z_{0n-\text{tube}} = Z_{c-\text{tube}}\dfrac{A_n+B_n}{A_n-B_n}$ $= Z_{c-\text{tube}}\dfrac{e^{2ik_nL}e^{2\gamma_nL}+\Gamma_{\text{tube}}}{e^{2ik_nL}e^{2\gamma_nL}-\Gamma_{\text{tube}}} \neq Z_{ca-\text{tube}}G_n e^{i\phi_n}$	$Z_{0n} = Z_{cn}\dfrac{A_n-B_n}{A_n+B_n}$ $= Z_{cn}\dfrac{e^{2ik_nL}e^{2\gamma_nL}-\Gamma_n}{e^{2ik_nL}e^{2\gamma_nL}+\Gamma_n} = Z_{cn}G_n{}^{-1}e^{-i\phi_n}$

$$\Gamma_{n-\text{tube}} = \frac{R_L}{2Z_{c-\text{tube}}+R_L+2Z_{c-\text{tube}}n\omega CR_L i} = \Omega_{n-\text{tube}}e^{i\theta_{n-\text{tube}}} \tag{45b}$$

As to a pure resistor, there is no phase shift between the forward and reflected waves at $x=L$. In contrast, a three-element Windkessel model gives rise to the phase shift of the nth reflected wave relative to the nth forward wave

$$\theta_{n-\text{tube}} = -a\tan\frac{2Z_{c-\text{tube}}n\omega R_L C}{2Z_{c-\text{tube}}+R_L}\ (q_{n-\text{tube}}<0) \tag{46}$$

Input impedance is written as

$$Z_{0n-\text{tube}} = Z_{c-\text{tube}}\frac{A_n+B_n}{A_n-B_n} = Z_{c-\text{tube}}\frac{e^{2ik_nL}e^{2\gamma_nL}+\Gamma_{n-\text{tube}}}{e^{2ik_nL}e^{2\gamma_nL}-\Gamma_{n-\text{tube}}} = Z_{c-\text{tube}}G_n e^{i\phi_n} \quad \text{with} \quad \frac{A_n+B_n}{A_n-B_n} = G_n e^{i\phi_n} \tag{47}$$

Thus, a pure resistor and a three-element Windkessel model cannot be equal to the nth normalized input impedance

$$\frac{e^{2ik_nL}e^{2\gamma_nL}+\Gamma_{n-\text{tube}}}{e^{2ik_nL}e^{2\gamma_nL}-\Gamma_{n-\text{tube}}} \neq G_n e^{i\phi_n} \tag{48}$$

Table 2 summarizes the difference between the tube-load model with a three-element Windkessel model as the load and the vibrating-string model. Since a pure resistor load is totally physiologically unrealistic (see Sec. 5), it is not included in the table.

4.3 Difference in Input Power at the Aorta and Driving Force on the Left Ventricle. Based on the tube-load model, the input power at the aorta is calculated as

$$P_{n-\text{tube}} = \frac{1}{2}\Delta p_n Q_n = \frac{1}{2}\left[\frac{2\eta_{afn}}{G_n e^{i\phi_n}+1}\right]^2 \frac{4\pi\rho_b c_n^3}{1-F_{10}}G_n e^{i\phi_n} \tag{49}$$

Note that the measured input impedance and harmonics-dependent wall shear stress are incorporated in this equation. Equation (49) does not distinguish the input power between the arterial wall and blood flow and is not related to $(n\omega)^2$, as shown in Eq. (35*b*). This input power from the tube-load model is included in Table 1 for comparison. Based on the tube-load model, the driving force $F_{\text{tube}}(t)$ on the LV for blood velocity becomes [12]

$$F_{\text{tube}}(t) = \sum_n \left\{ D + i\left(Mn\omega - \frac{K}{n\omega}\right) + \text{Re}(Z_{0n-\text{meas}})(\pi a^2)^2 + i\,\text{Im}(Z_{0n-\text{meas}})(\pi a^2)^2 \right\} \frac{2c_0}{a}\left(\eta_{afn}e^{in\omega t} - \eta_{abn}e^{in\omega t}\right) \tag{50}$$

5 Discussion

In the tube-load model [2–7], the distributed 1D model [1], and related clinical studies on the CV system [1], Eq. (38) is the theoretical basis for defining the parameters that relate wave transmission and reflection to arterial properties and geometries. Pulsatile pressure and blood flow rate are defined as driving force and velocity, respectively, as shown in Table 2. Then, the ratio of pulsatile pressure versus blood flow rate (without wave reflection) becomes characteristic impedance. Yet, since Eq. (38) does not comply with the standard 1D wave equation, these definitions are not consistent with their counterparts in the context of 1D wave propagation, and their physical implications to wave transmission and reflection are then obscured. Built on the standard 1D wave equation, the vibrating-string model for the arterial tree allows defining of all the parameters consistent with their well-established physical implications in the acoustical field [12], which can be directly adopted for studying wave transmission and reflection in the aorta-periphery section.

Other than the difference in definitions of the parameters and their physical implications between the tube-load model and the vibrating-string model, the vibrating-string model is further utilized to derive theoretical relation of load impedance to input impedance, which reveals that 1) input impedance is a dependent parameter and is determined by load impedance and arterial properties and geometries and 2) the use of a three-element Windkessel model as the load stipulates harmonics-dependence of load impedance, which is inconsistent with the measured input

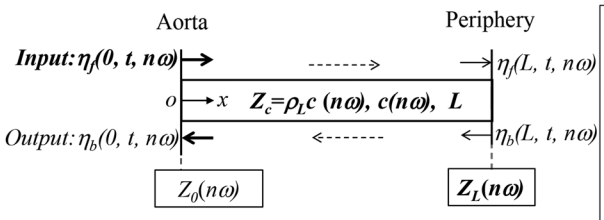

$$Z_{0n} = Z_{cn}\frac{\eta_{afn}-\eta_{abn}}{\eta_{afn}+\eta_{abn}} = Z_{cn}\frac{Z_{cn}(e^{2ik_nL}e^{2\gamma_nL}-1)+Z_{Ln}(e^{2ik_nL}e^{2\gamma_nL}+1)}{Z_{cn}(e^{2ik_nL}e^{2\gamma_nL}+1)+Z_{Ln}(e^{2ik_nL}e^{2\gamma_nL}-1)}$$

Note: $c(n\omega)$ determines k_n *and* γ_n; η_{afn} and η_{abn} denote the nth forward and reflected amplitudes at the aorta, respectively.

Independent parameters

Transmission characteristics (arterial properties and geometries): $Z_c=\rho_L c(n\omega)$, $c(n\omega)$, L, $Z_L(n\omega)$

Pulsatile parameter: $\eta_f(0, t, n\omega)$

Dependent parameters

Input impedance: $Z_0 \propto Z_c=\rho_L c(n\omega)$, $c(n\omega)$, L, $Z_L(n\omega)$

Pulsatile parameters: $\eta_b(0, t, n\omega)$, $\eta_f(L, t, n\omega)$, $\eta_b(L, t, n\omega)$

Input: $\eta_f(0,t,n\omega) = \sum_n \eta_{afn} e^{in\omega t}$

Output: $\eta_b(0,t,n\omega) = \sum_n \frac{Z_{cn}-Z_{Ln}}{Z_{cn}+Z_{Ln}} e^{-2ik_nL} e^{-2\gamma_nL} \eta_{afn} e^{in\omega t} = \sum_n \frac{Z_{cn}-Z_{0n}}{Z_{cn}+Z_{0n}} \eta_{afn} e^{in\omega t}$

Fig. 4 The vibrating-string model for closed-loop wave transmission and reflection in the arterial section between the aorta and periphery: the forward waveform $\eta_f(0,t,n\omega)$ at the aorta as the input transmits to periphery, is reflected at periphery, and transmits back as the reflected waveform $\eta_b(0,t,n\omega)$ at the aorta as the output, with independent parameters in bold font and dependent parameters in unbold font

impedance. Moreover, theoretical expressions for return time and reflection magnitude at each harmonic are derived in terms of input impedance and can be calculated based on the measured input impedance.

5.1 Who Are Independent Parameters and Dependent Parameters in Closed-Loop Wave Transmission and Reflection Between the Aorta to Periphery? Since the aorta is at the start of the arterial tree, it is commonly assumed that aortic pressure waveform is the input and peripheral pressure waveform is the output in the tube-load and distributed 1D models [1–7]. As shown in Eq. (25), since aortic reflected pressure waveform is affected by all the downstream parameters, it should not be included in the input. As shown in Fig. 4, by following the wave transmission path, the input and the output and the role of all the parameters become clear. The input is aortic forward waveform $\eta_f(0,t,n\omega)$, which is not affected by the downstream parameters (Note that the LV is excluded here.), and is a collection of harmonics ($n\omega$) of the heartbeat. This forward waveform transmits toward periphery, with transmission characteristics (i.e., Z_c, c, and L) determined by arterial properties and geometries. At periphery, the forward waveform $\eta_f(L,t,n\omega)$ is reflected with load impedance Z_L. The reflected waveform $\eta_b(L,t,n\omega)$ transmits toward the aorta with the same transmission characteristics, and becomes the reflected waveform at the aorta $\eta_b(0,t,n\omega)$, which is the output. Given its influence on small arteries, the fluid-loading term F_{10} should not be neglected in the aorta-periphery section, and thus harmonics-dependence of wave velocity and characteristic impedance needs to be included in reconstruction of aortic pressure waveform.

Although input impedance Z_0 can be calculated from pulsatile parameters at the aorta using Eq. (31), it is determined by transmission characteristics and load impedance, as expressed in Eq. (20). Thus, Z_0 is not an independent parameter. Then, four parameters: Z_c, c, L, and Z_L, are needed to reconstruct aortic pressure waveform from peripheral pressure waveform with accurate representation of the harmonics of aortic pressure waveform. In clinical studies, aortic pressure waveform and blood flow waveform are measured to separate aortic forward waveform from aortic reflected waveform and also calculate Z_0. Certainly, measurement at the aorta involves high cost and great technical complexity. In contrast, measurement of peripheral pressure waveform can be easily achieved using a tactile sensor or a photoplethysmographic (PPG) sensor [2–7]. However, measurement of blood flow waveform at peripheral arteries becomes challenging, due to their small size. As such, it is difficult, if not impossible, to measure Z_L. As analyzed here, the measured Z_0 can be utilized to obtain Z_L.

Following the wave transmission path leads to closed-loop wave transmission and reflection between the aorta and periphery: wave transmission starts and ends at the aorta, and wave reflection at the aorta is a combination of round-trip wave transmission and wave reflection at periphery. This closed-loop wave transmission and reflection reveals that the input and the output are both at the aorta and why input impedance is not an independent parameter but depends on load impedance and transmission characteristics. This is important, in the sense that the reflected waveform at the aorta is not an independent parameter, but depends on the forward waveform and load impedance, and transmission characteristics. Then, three clinical indices at the aorta are indicative of load impedance and transmission characteristics, as well as harmonics of the forward waveform. As compared with following the whole waveform along the arterial tree, closed-loop wave transmission and reflection serves better for revealing the entangled relations of input impedance, load impedance, and harmonics in the aorta-periphery section. As seen in Sec. 3, relating input impedance to load impedance allows the calculation of return time and reflection magnitude at the aorta using input impedance, since the latter manifests round-trip wave transmission and wave reflection at periphery.

5.2 Characteristic Impedance and Load Impedance Versus Tapered Arterial Geometry. In the context of 1D wave propagation, characteristic impedance has defined the ratio of driving force versus velocity [12]. In this regard, the definition of characteristic impedance in clinical studies and in the tube-load model is not correct, in the sense that pulsatile pressure is not driving force, and blood flow rate is not velocity. The arterial tree contains multiple arterial segments with a relatively sudden radius change at segment connects [1,2,9]. Furthermore, an arterial segment contains a tapered geometry (slowly reduced radius from the entrance to the exit) [1,2,7,9]. Here, the effect of the arterial geometrical change on wave reflection is examined via characteristic impedance and load impedance.

It is well established that any change in characteristic impedance (or impedance mismatch) along the wave transmission path causes wave reflection [12]. If one arterial segment with artery radius a_1 and wave velocity c_1 is followed by another arterial segment with a_2 and c_2. The change in characteristic impedance causes wave reflection to happen at the segment connect, with the following reflection coefficient [12]

$$\Gamma = \frac{Z_{c1}-Z_{c2}}{Z_{c1}+Z_{c2}} = \frac{1-\frac{c_2\pi a_2^2}{c_1\pi a_1^2}}{1+\frac{c_2\pi a_2^2}{c_1\pi a_1^2}} \tag{51}$$

As far as there is a reduction in arterial radius at a location, there exists impedance mismatch and then wave reflection occurs [12].

This equation explains wave reflection taking place everywhere along the length of a tapered arterial segment, which is observed in the tapered tube-load and the distributed 1D models [1]. Thus, the forward and reflected waves measured at an artery site need to be treated as the compound forward and reflected waves, which result from wave reflection at multiple sites in the arterial tree [1].

Load impedance at periphery Z_L results from 1) impedance mismatch between the aorta-periphery section and rest arteries and 2) boundary conditions at termination [13]. Neither a pure resistor nor a three-element Windkessel model is capable of capturing these two factors. In the context of the 1D wave propagation, $\mathrm{Re}(Z_L)$ presents the part of energy transmitted to rest arteries and $Im(Z_L)$ represents the part of energy reflected back to the aorta-periphery section [12]. A pure resistor as Z_L indicates no wave reflection at periphery, which is physiologically unrealistic. Furthermore, this pure resistor gives rise to harmonic-independence of Z_L. Combination of Eqs. (44*a*) and (48) explains the oscillation of input impedance with harmonics, which is observed in the tube-load model with a pure resistor as the load [1]. The Windkessel model as Z_L allows wave reflection and harmonics-dependence. However, the dependence of Z_L on harmonics is stipulated by the values of the three elements, as shown in Eq. (44*b*). It is well known in the acoustical field that a tapered geometry causes the dependence of boundary conditions on harmonics [12]. Owing to mathematical complexity, an explicit expression on harmonics-dependence of boundary conditions for a tapered geometry is unavailable. Anatomical complexity in the arterial tree exacerbates difficulty in attaining harmonic-dependence of boundary conditions at termination. However, As shown in Fig. 4, harmonics-dependence of Z_L can be obtained from the measured Z_0 in clinical studies.

5.3 Measured Input Impedance, Return Time, Reflection Magnitude, and Augmentation Index Versus Harmonics. Based on Fig. 4, input impedance is determined by load impedance and arterial properties and geometries in the aorta-periphery section. Although harmonics-dependence of wave velocity and characteristic impedance in the aorta-periphery section is clear, harmonics-dependence of load impedance is unknown, as explained in Sec. 5.2. Thus, how the input impedance varies with harmonics can only be obtained from the measured values. As an example, the measured harmonics of pulsatile pressure and blood flow waveform at the aorta in the literature [8], as shown in Figs. 5(*a*) and 5(*b*), are used to calculate the measured input impedance based on Eq. (31). The variation of the measured input impedance with harmonics is plotted in Fig. 5(*c*). Harmonics-dependence of load impedance can then be estimated from Eq. (23*b*).

It is found in clinical studies that the measured return time of the reflected waveform $\eta_{ab}(t)$ is longer than $2L/c_0$ [1]. As shown in Eq. (26*b*), the complex value of Z_L leads to a phase delay and thus extra time delay. Since it is found that return time depends little on c_0 in clinical studies [1], it might indicate that high arterial stiffness leads to a higher θ_n at periphery. Because Z_L and round-trip wave transmission are embedded in Z_0, input impedance Z_0 is allowed to estimate reflection magnitude and return time. As shown in Fig. 6(*a*), reflection magnitude varies with harmonics, and reflection magnitude for the whole waveform is not the average of the ten harmonics. As expressed in Eq. (28), reflection magnitude of the whole waveform is determined by not only Z_L (or Z_0) but also harmonics of the forward waveform. As shown in Fig. 6(*b*), due to harmonics-dependence of phase delay at periphery and wave velocity, the reflected waves of different harmonics arrive at the aorta at different return times. As shown in Fig. 7, harmonics-dependence of return time makes it elusive to identify the foot of the reflected waveform [1,14]. Defined as the ratio of augmented pressure to pulsatile pressure, AP/PP [1,14], AI varies greatly with the location of this foot. As a composite indicator of return time and reflection magnitude, AI also manifests harmonics of aortic pressure waveform. Since return

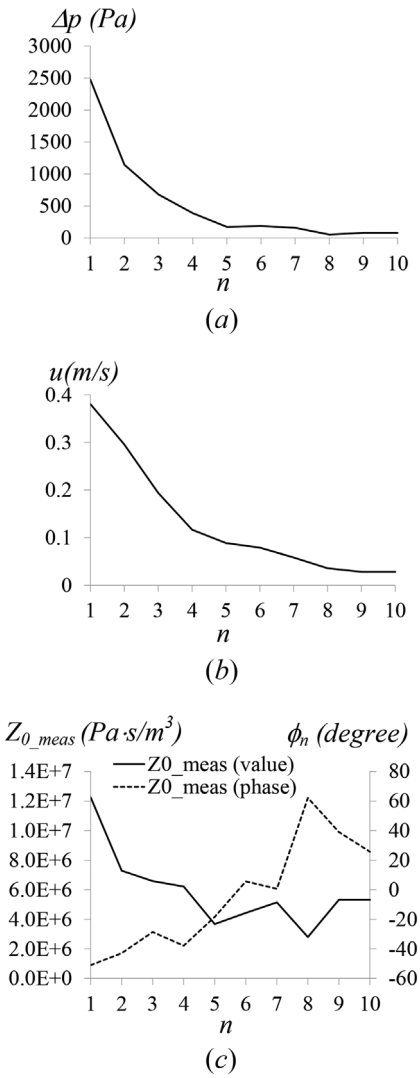

Fig. 5 Harmonics of: (*a*) pulsatile pressure, (*b*) blood velocity at the aorta, and (*c*) measured input impedance varies with harmonics in Ref. [8]

time, reflection magnitude, and AI are all affected by harmonics of aortic pressure waveform, the reconstructed aortic pressure waveform needs to capture accurate harmonics information for accurate estimates of these clinical indices. Given the dependence of return time and reflection magnitude on arterial stiffness (i.e., c_0), arterial radius, as well as harmonics, it is no surprise that AI carries independent clinical values, as compared with arterial stiffness [2,5]. Taken together, the definitions of return time for the whole waveform and AI are inconsistent with harmonics-dependence of return time, and reflection magnitude for the whole waveform and AI carry harmonics information of aortic pressure waveform. Given the dominance of the 1st harmonic in aortic pressure waveform, reflection magnitude and return time of the 1st harmonic might serve better as clinical indices for arterial properties and geometries and wave reflection at periphery, and harmonics of the whole waveform might serve as a clinical index indicative of the LV function, instead of AI.

5.4 The Left Ventricle-Artery Interaction for Driving Force on the Left Ventricle and Harmonics of Aortic Pressure Waveform. To calculate the driving force on the LV based on the lumped-element model, input impedance defined in the vibrating-string model is calculated from the measured input impedance, as shown in Fig. 8. Based on the harmonics of aortic pressure waveform in Fig. 5(*a*), the two driving forces on the LV is

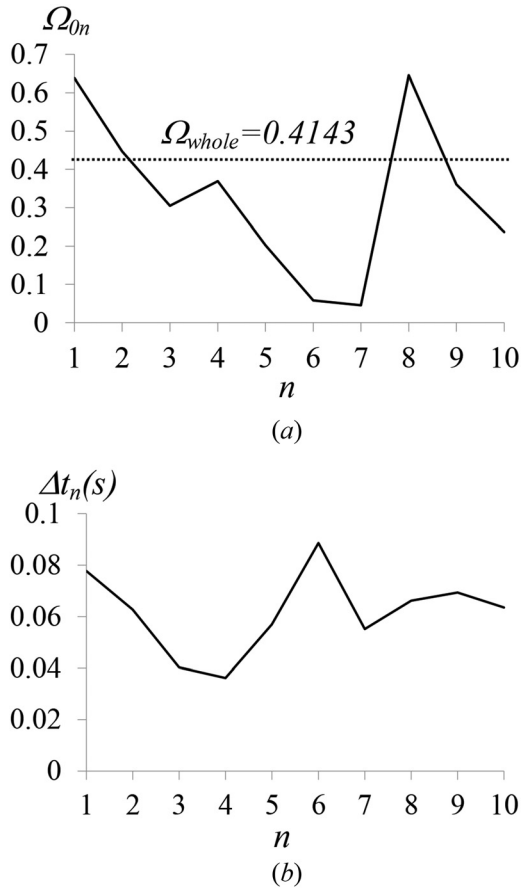

Fig. 6 Harmonics-dependence of: (*a*) return time and (*b*) reflection magnitude, based on the measured input impedance in Fig. 5(*c*)

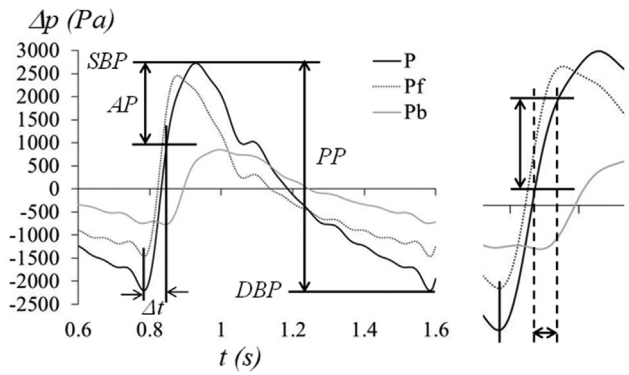

Fig. 7 Definition of AI and difficulty in identifying the foot of the backward waveform, due to harmonics-dependence of return time (P: pulsatile pressure waveform (Ref. [8]), Pf: forward pressure waveform, and Pb: reflected pressure waveform)

calculated from Eq. (36*a*) and Eq. (36*b*) and are plotted in Figs. 9(*a*) and 9(*b*). The value of M for the LV is chosen to be 0.3 kg (close to the mass of the heart), and the value of K is chosen such that the LV operates at resonance at the heartbeat. It is assumed that the LV operates with high efficiency so that the value of D is very small. Figure 10(*a*) compares the phases of blood velocity, radial wall displacement (or pulsatile pressure), and $F_u(t)$. It is interesting to note that $F_u(t)$ is similar to the waveform of an ECG signal to some extent [15] and is also ahead of blood velocity, similar to an ECG signal. Figure 9(*c*) shows the calculated driving force based on Eq. (50), which is completely different from the waveform of an ECG signal. As shown in Fig. 10(*b*), this driving

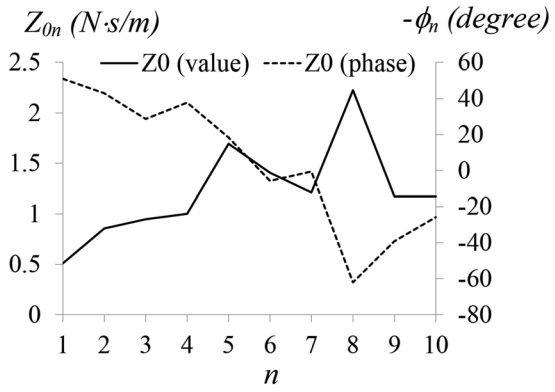

Fig. 8 Input impedance in the vibrating-string model based on the measured input impedance in Fig. 5(*c*)

force is in phase with blood velocity. As such, the tube-load model might not be suitable for studying the LV-artery interaction for relating aortic pressure waveform to the LV function.

As shown in Fig. 3, the LV and the arterial tree and its termination all play a role in determining harmonics of $\eta_a(t)$. It is well established in the musical instruments field [16] that the excitation source (e.g., a soft hammer versus a rigid hammer), Z_c in the vibrating string, and Z_L at the other end of the string will affect the interaction between the excitation source and the vibrating string, and consequently the generated harmonic amplitude percentages of $\eta_a(t)$ at different n-levels. With the excitation source at one end, the generated harmonics of $\eta_a(t)$ usually contain a decreasing trend of amplitude percentages with higher n-levels [16], as shown in Fig. 5(*a*). Given the role of the LV in determining harmonics of aortic pressure waveform and the role of harmonics in AI, it is no surprise that AI is found to manifest not only arterial properties and geometries but also the LV function [17].

The model for the LV-artery interaction in Fig. 3 is a rather simplified model to relate the LV to the arterial tree. Similar to hammer-string interaction in a piano [16], it is exceedingly intricate to capture the LV-artery interaction for predicting harmonics of aortic pressure waveform. Generally speaking, low Zc increases the amplitudes of higher harmonics, while high Zc increases the amplitudes of lower harmonics [18]. Higher harmonics lead to higher amplitudes of wall shear stress, as compared with lower harmonics [10]. This may explain the importance of accurate representation of higher harmonics in reconstructed aortic pressure waveform, which dictates the peak wall stress in the LV, with the latter being a fundamental biophysical driver of myocardial hypertrophy [5].

5.5 Machine-Learning Techniques for Reconstruction of Aortic Pressure Waveform. In the studies of the tube-load model, machine learning techniques have focused on optimizing the values of load impedance to improve accuracy in reconstructed aortic pressure waveform from its peripheral counterpart, to the neglect of physical implications of load impedance and without examining the input impedance [2–7]. This explains why a pure resistor is used as the load [4] and a generic pole–zero model for the load [3] is considered to carry no physiological meaning. Since a pure resistor is inconsistent with wave reflection, it is impossible to extract physiological meaning from the obtained results based on it [1,4]. This work shows that the essence of these machining-learning techniques is about chasing physiologically realistic harmonic-dependence of load impedance [3,5]. Yet, given that at least 20 unknown values (if only the first ten harmonics are utilized.) are needed for accurate representation of harmonic-dependence of load impedance, there are a great many combinations of the 20 values to match the reconstructed one with the measured one. Taken together, the results derived from

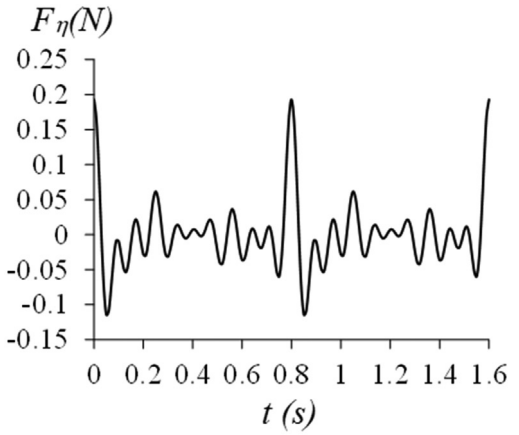

(a)

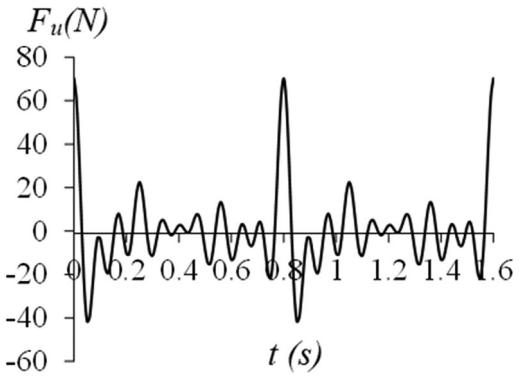

(b)

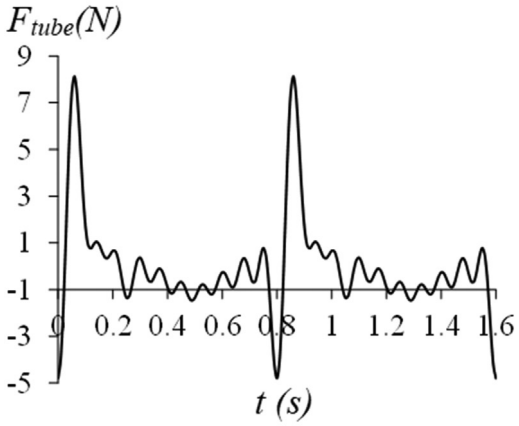

(c)

Fig. 9 Driving force on the LV based on the vibrating-string models for: (*a*) radial wall displacement and (*b*) blood velocity and based on the tube-load model (Note: $M = 0.3$ kg, $K = M{\cdot}\omega^2$, and $D = \sqrt{KM}/Q$ with $Q = 100$ are used for calculation)

application of machine-learning techniques to reconstruction of aortic pressure waveform do not carry much physiological meaning unless the application is consistent with the associated theories and physical implications.

5.6 Study Limitations. In this work, the aorta-periphery section is treated as a uniform vibrating string with the same arterial geometries and properties. This treatment neglects the following three factors: 1) tapered arterial geometry and nonuniform arterial properties in an arterial segment, 2) different geometries and properties among multiple arterial segments, and 3)

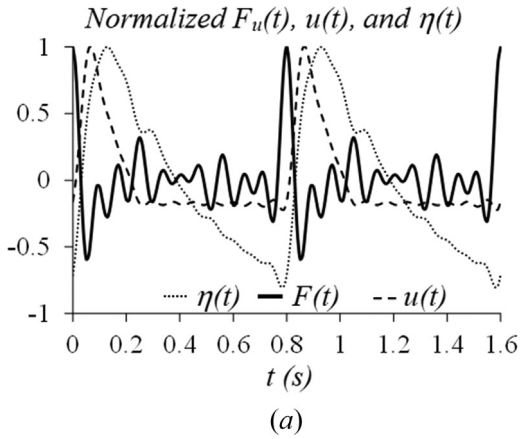

(a)

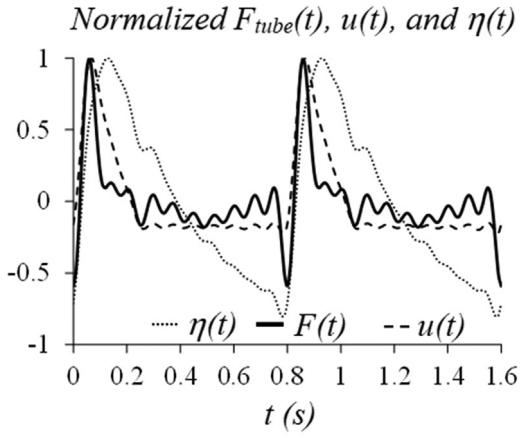

(b)

Fig. 10 Normalized driving force on the LV and normalized blood velocity and radial wall displacement at the aorta based on: (*a*) the lumped-element mechanical model for the LV-artery interaction and (*b*) the tube-load model

bifurcations. These neglected factors are identical to those for the uniform tube-load model and those for the calculation of PWV in clinical studies [1–3]. However, as compared with the tube-load model and PWV in clinical studies, harmonics-dependent wall shear stress is included in this work, given that it causes non-negligible dependence of wave transmission and reflection on harmonics and thus greatly affects aortic pressure waveform.

By neglecting the tapered arterial geometry and nonuniform arterial properties in an arterial segment, repeated wave reflection and continuously-changing wave velocity along the length of an arterial segment are omitted, as discussed in Sec. 5.2. By neglecting different geometries and properties among multiple arterial segments, all the arterial segments retain the same wave velocity and the same characteristic impedance, and no wave reflection occurs at segment connects. By neglecting bifurcations, their complicate effect on wave reflection is omitted. It is worth mentioning that bifurcations have recently been modeled as springs at the ends of an arterial segment, and spring coefficients are adjusted for matching pulsatile pressure waveforms in the segment [19]. It is unknown whether the effect of these neglected factors on wave reflection is harmonics-dependent. By combining Eqs. (32) and (20), the measured input impedance is related to load impedance (or reflection coefficient) by

$$\frac{\left(\frac{\rho_b c_n}{\pi a^2}\right)_{\text{aorta}}}{Z_{0n\_\text{meas}}} = \frac{Z_{cn}(e^{2ik_nL}e^{2\gamma_nL} - 1) + Z_{Ln}(e^{2ik_nL}e^{2\gamma_nL} + 1)}{Z_{cn}(e^{2ik_nL}e^{2\gamma_nL} + 1) + Z_{Ln}(e^{2ik_nL}e^{2\gamma_nL} - 1)} = \frac{e^{2ik_nL}e^{2\gamma_nL} - \Gamma_n}{e^{2ik_nL}e^{2\gamma_nL} + \Gamma_n} \tag{52}$$

Since the measured input impedance captures the effect of the neglected factors on wave reflection and load impedance, the effect of the neglected factors on wave reflection is factored in load impedance in Eq. (52). In clinical studies, pulsatile pressure waveform is treated as one forward waveform and one reflected waveform for extracting clinical measures, without considering repeated wave reflections at multiple sites. The uniform vibrating-string model also neglects repeated wave reflection and provides one forward waveform and one reflected waveform. Finally, arterial properties and geometries in the vibrating-string model need to take equivalent values for accounting for their variations among multiple arterial segments.

6 Conclusion

In light of reconstruction of aortic pressure waveform with accuracy for its clinical indices, a vibrating-string model is developed to examine the roles of input impedance, load impedance, and harmonics in aortic pressure waveform and its three clinical indices. On the one hand, the revealed role of the three parameters in the clinical indices identifies the importance of physiologically realistic load impedance in reconstruction of aortic pressure waveform with accuracy. On the other hand, this work reveals physical implications and physiological implications of the three clinical indices and identifies a lack of consideration of harmonics-dependence of wave transmission and reflection in their definitions. Harmonics of aortic pressure waveform is suggested as a clinical index indicative of the LV function, instead of AI.

This work provides a theoretical guidance for reconstruction of aortic pressure waveform and interpretation of aortic pressure waveform for assessing arterial health and the LV function. The key insights shed by this work on reconstruction of aortic pressure waveform and its associated physical implications are summarized here:

(1) Load impedance must be complex, with the real part representing energy transmitted and the imaginary part representing energy reflected back. Complex load impedance translates to non-zero phase angle of reflection coefficient, which represents the phase delay of the reflected wave relative to the forward wave at periphery and affects return time at the aorta.
(2) A three-element Windkessel model in the tube-load model stipulates harmonic-dependence of load impedance, which is inconsistent with physiological realities.
(3) Input impedance is a dependent parameter, and is determined by load impedance and arterial geometries and properties. Physiologically realistic harmonic-dependence of load impedance can only be obtained from the measured input impedance, instead of machine-learning techniques. Return time at the aorta can be estimated from input impedance, due to the dependence of input impedance on load impedance.
(4) To capture the LV-artery interaction for aortic pressure waveform, the arterial tree and its termination need to be treated with the real part of input impedance as a damper and the imaginary part of input impedance as a spring. Together with arterial properties and geometries, the LV plays a role in determining harmonics of aortic pressure waveform.
(5) Fluid loading causes harmonic-dependence of wave velocity and characteristic impedance. Accordingly, each harmonic has its own return time and reflection magnitude at the aorta. Meanwhile, harmonics of the forward pressure waveform at the aorta are non-uniform. As such, harmonics of aortic pressure waveform play an important role in determining the three clinical measures: return time, reflection magnitude, and AI. AI carries much more physiological information than arterial stiffness, and is indicative of the LV function.

Based on this work, it might be more practical to develop a better understanding of harmonic-dependence of input impedance and harmonics of the forward pressure waveform at the aorta for different groups of population, based on the measured blood flow rate and the measured aortic pressure waveform, prior to reconstruction of aortic pressure waveform from peripheral counterpart for estimates of its clinical measures using a 1D model.

Funding Data

- Directorate for Engineering (Funder ID: 10.13039/100000084).

Data Availability Statement

The authors attest that all data for this study are included in the paper.

References

[1] Westerhof, B. E., and Westerhof, N., 2018, "Uniform Tube Models With Single Reflection Site Do Not Explain Aortic Wave Travel and Pressure Wave Shape," Physiol. Meas., **39**(12), p. 124006.
[2] Zhou, S., Xu, L., Hao, L., Xiao, H., Yao, Y., Qi, L., and Yao, Y., 2019, "A Review on Low-Dimensional Physics-Based Models of Systemic Arteries: Application to Estimation of Central Aortic Pressure," Biomed. Eng. Online, **18**(1), p. 41.
[3] Zhang, G., Hahn, J. O., and Mukkamala, R., 2011, "Tube-Load Model Parameter Estimation for Monitoring Arterial Hemodynamics," Front. Physiol., **2**, p. 72.
[4] Gao, M., Rose, W. C., Fetics, B., Kass, D. A., Chen, C. H., and Mukkamala, R., 2016, "A Simple Adaptive Transfer Function for Deriving the Central Blood Pressure Waveform From a Radial Blood Pressure Waveform," Sci. Rep., **14**(6), p. 33230.
[5] Du, S., Liu, W., Yao, Y., Sun, G., He, Y., Alastruey, J., Xu, L., Yao, Y., and Qian, W., 2022, "Reconstruction of the Aortic Pressure Waveform Using a Two-Level Adaptive Transfer Function Strategy," Measurement, **204**, p. 112111.
[6] Ebrahimi, N. S., Carey, J. P., McMurtry, M. S., and Hahn, J. O., 2017, "Model-Based Cardiovascular Disease Diagnosis: A Preliminary in-Silico Study," Biomech. Model Mechanobiol., **16**(2), pp. 549–560.
[7] Mousavi, A., Tivay, A., Finegan, B., McMurtry, M. S., Mukkamala, R., and Hahn, J. O., 2019, "Tapered vs. Uniform Tube-Load Modeling of Blood Pressure Wave Propagation in Human Aorta," Front. Physiol., **10**, p. 974.
[8] Qureshi, M. U., Colebank, M. J., Schreier, D. A., Tabima, D. M., Haider, M. A., Chesler, N. C., and Olufsen, M. S., 2018, "Characteristic Impedance: Frequency or Time Domain Approach?," Physiol. Meas., **39**(1), p. 014004.
[9] Westerhof, N., and Westerhof, B. E., 2012, "Wave Transmission and Reflection of Waves "the Myth is in Their Use," Artery Res., **6**(1), pp. 1–6.
[10] Hao, Z., Rahman, M. M., Jutlah, L. B. L., Athaide, C. E., and Au, J. S., 2023, "Axial Wall Displacement at the Common Carotid Artery is Associated With the Lamb Waves," ASME J. Med. Diagn., **6**(1), p. 011008.
[11] Womersley, J. R., 1955, "XXIV. Oscillatory Motion of a Viscous Liquid in a Thin-Walled Elastic Tube—I: The Linear Approximation for Long Waves," Lond. Edinb. Dublin Philos. Mag. J. Sci., **46**(373), pp. 199–221.
[12] Kinsler, L. E., Frey, A. R., Coppens, A. B., and Sanders, J. V., 2000, *Fundamentals of Acoustics*, 4th ed., Wiley, Hoboken, NJ.
[13] Wang, J. J., and Parker, K. H., 2004, "Wave Propagation in a Model of the Arterial Circulation," J. Biomech., **37**(4), pp. 457–70.
[14] Afkhami, R., and Johnson, S., 2021, "Wave Reflection: More Than a Round Trip," Med. Eng. Phys., **92**, pp. 40–44.
[15] Zhu, Q., Tian, X., Wong, C. W., and Wu, M., 2021, "Learning Your Heart Actions From Pulse: ECG Waveform Reconstruction From PPG," IEEE Internet Things J., **8**(23), pp. 16734–16748.
[16] Raichel, D. R., 2006, *The Science and Applications of Acoustics*, Springer Science & Business Media, Berlin.
[17] Heusinkveld, M. H. G., Delhaas, T., Lumens, J., Huberts, W., Spronck, B., Hughes, A. D., and Reesink, K. D., 2019, "Augmentation Index is Not a Proxy for Wave Reflection Magnitude: Mechanistic Analysis Using a Computational Model," J. Appl. Physiol., **127**(2), pp. 491–500.
[18] Chen, P. J., Wu, H. K., Hsu, P. C., Lo, L. C., and Chang, H. H., 2020, "Effects of Five Daily Activities on Harmonic Analysis of the Radial Pulse," Evid. Based Complement. Altern. Med., **2020**, p. 6095674.
[19] Tokunaga, T., Mori, K., Kadowaki, H., and Saito, T., 2020, "Study on Natural Vibration Characteristics Based on the Coupled Wave Theory of Spring Supported Elastic Pipes and Fluids," ASME Paper No. IMECE2020-23742.